Instabilities of a spin-valve system with perpendicular polarizer and in-plane bias field

J. H. Chang,* H. H. Chen, and C. R. Chang†
Department of Physics, Center for Theoretical Physics, and Center for Quantum Sciences and Engineering, National Taiwan University, Taipei 10617, Taiwan
(Received 7 September 2010; published 22 February 2011)

Under a perpendicular spin-transfer-torque (STT) polarizer and in-plane (IP) bias magnetic field, three-dimensional instability thresholds of the critical strength of STT and the field are derived from an effective one-dimensional free energy. The modified astroids derived from the STT and IP fields are quite different from the classical Stoner-Wohlfarth astroid. We find that the STT breaks the symmetry of the astroid seriously when the orientation of bias field is along the easy and hard axes. In particular, the modified astroid not only separates the region with two stable states from the region with only one stable state, but also delimits the region with a dynamical stable state (no stable equilibrium state) when the amplitude of the STT is larger than a critical value required to switch the magnetization at zero-bias field. Finally, the nucleation field, coercivity, and precessional critical field for uniaxial anisotropy are rigorously determined including the effect of the STT, and the hysteresis loops for various orientations of a bias field are computed and discussed.

DOI: 10.1103/PhysRevB.83.054425 PACS number(s): 75.75.−c, 72.25.−b, 75.60.−d, 85.75.−d

I. INTRODUCTION

Recently most research has been performed for a spin-valve system[1–18] or a magnetic tunnel junction structure.[19–22] In a spin-valve system, it is known that a "perpendicular-to-plane (PERP) polarizer" used in spin valves has attracted considerable interest because of great potential applications for new types of spintronic devices, such as magnetic random access memory and rf devices.[12–18] The PERP polarizer is usually composed of a Pt/$(Co/Pt)_5$ multilayer structure with strong out-of-plane anisotropy and a Co/Cu/Co layer with a strong spin polarization.[15] In a PERP device (see Fig. 1), when a current flows perpendicularly through two magnetic layers separated by a thin nonmagnetic spacer layer (metallic junction), the current becomes spin polarized by transmission through or upon reflection from the first magnetic layer (polarizer layer), therefore, it carries angular momentum along the orientation of the first magnetization, which is perpendicular to the film plane of the second magnetic layer (free layer). The nonmagnetic layer is thin enough, and thus the polarized current retains its polarization so that the angular momentum carried by the current can interact with the free-layer magnetization. This is a spin-transfer-torque (STT) effect[23,24] and can be used to induce either a steady-state precession at large angle or a irreversible reversal to a new stable equilibrium state.

Theoretically, it has been reported that the PERP-polarizer-based spin valve can realize fast and low-power-consuming magnetization switching. However, there are also some disadvantages, such as the necessity for precise controllability of the current pulse and read-before-write in the data storage procedure.[13,14] Recently, a different process of magnetization switching is proposed by Morise and Nakamura.[17] Both the PERP polarizer and the magnetic field are simultaneously employing and is usually called relaxing-precessional switching. It offers an easier, faster, and lower-power consuming way to manipulate the magnetization state.

Even though the magnetization reversal is a complicated physical problem, some ideal cases have been well studied. Several reversal modes were found under different conditions, such as curling and buckling, which are nonuniform modes in bulk materials.[25] Aharoni has indicated that for large magnetic particles, the preferred mechanism is curling, while for small ones coherent rotation is preferred.[26] Below a critical dimension of the magnetic particles, the most favorable energy state of a nanosized object is a single domain, i.e., Stoner-Wolhfarth (SW) particles.[27] Recent advances in the technological environment make the fabrication and probing of nanosized particles realizable. In the SW model, the magnetization switching constraints of the coherent rotation of a single-domain particle constructs an astroid curve called the SW limit, which indicates the angular dependence of the minimal switching field. The SW astroid was derived from an instability analysis,[28,29] and its easy geometric criteria have provided guidelines for material fabrication engineers and guidelines for writing schemes for head designers in the past decades. Another relaxational reversal of magnetization had been reported to have a lower coercivity than the Stoner-Wohlfarth limit.[30]

Similarly, the magnetization switching induced by the STT, together with an applied magnetic field, is expected to have similar parametric constraints. The modified astroid was examined by previous researchers in the case of an in-plane (IP) polarized current and an IP magnetic field acting with a magnetization.[31,32] Because the STT generated from an IP polarizer is a nonconservative torque, such as the damping torque, it usually changes the stability of the magnetization equilibria, but does not change the position of the equilibria.[33,34] For the PERP polarizer, spin torque transferring into the free layer is not only expected to be more efficient than for the IP polarizer, but also can change the positions of the magnetization equilibria in the low-energy region (easy plane).[18] Up to now only the relaxing-precessional switching assisted by a PERP polarizer and a magnetic field along easy and hard axes have been analyzed.[16,18] However, the instability thresholds under a PERP polarizer and an IP field with an arbitrary orientation were not studied completely.

In this paper, we construct a one-dimensional effective free energy in the presence of a STT generated from a PERP polarizer and an IP field. In Sec. II, we use the Landau-Lifshitz-Gilbert-Slonczewski equation to analyze the influence of the spin torque on the switching mechanism of

the magnetization. A parametric form of the locus of the minimal switching field was derived under the influence of the injected spin-polarized current. A three-dimensional critical surface of the instability conditions for the IP magnetic field and the injected polarized current have been constructed. We also compute the angular dependence of the critical field, i.e., nucleation field and coercive force and precessional critical field in Sec. III, and hysteresis loops in Sec. IV. Interesting reversal behaviors of the magnetization are found when the STT is considered. Finally, the summary is given in Sec. V.

II. THEORY

The magnetization dynamics of the free layer driven by the spin-polarized current and applied magnetic field is modeled by the Landau-Lifshitz-Gilbert equation, including the Slonczewski's spin-torque term:

$$\frac{d\mathbf{M}}{dt} = -\gamma(\mathbf{M}\times\mathbf{H}_{\text{eff}}) + \frac{\alpha}{M_S}\left(\mathbf{M}\times\frac{d\mathbf{M}}{dt}\right) + \frac{\gamma a_j}{M_S}\mathbf{M}\times(\mathbf{M}\times\mathbf{p}),$$

with

$$\mathbf{H}_{\text{eff}} = H_K(M_x/M_S)\mathbf{x} - 4\pi M_z\mathbf{z} + \mathbf{H}_a. \quad (1)$$

Here $\mathbf{M}$ is the magnetization vector of the free layer, M_S is the saturation magnetization, γ is the gyromagnetic ratio, α is Gilbert damping constant, $a_j = \hbar g(\pi/2)j/2eM_S d$ is the strength of the STT with polarization vector $\mathbf{p} = \mathbf{z}$, j is the current density, and d is the film thickness of the free layer. The current is defined to be positive when it flows from the polarizer to the free layer (see Fig. 1). Because the vector $\mathbf{M}$ is always perpendicular to the vector $\mathbf{p}$ while considering the static case,[27] the a_j is proportional to the spin-torque efficient factor $g(\pi/2)$. The first term of the effective magnetic field $\mathbf{H}_{\text{eff}}$ is the uniaxial anisotropy field with an anisotropy constant H_K, the second term is the demagnetization field, and the third term is the IP bias field [Eq. (2)]:

$$\mathbf{H}_a = H_a(\cos\beta\mathbf{x} + \sin\beta\mathbf{y}), \quad (2)$$

which makes an angle β with the easy axis. By parametrizing the magnetization vector $\mathbf{M}$ in terms of the spherical coordinates (θ,ϕ), i.e., $\mathbf{M} = M_S(\sin\theta\cos\phi, \sin\theta\sin\phi, \cos\theta)$, Eq. (1) can be rewritten in the following autonomous form:

$$\dot{\theta} = f_1(\theta,\phi) + \alpha f_2(\theta,\phi),$$
$$\dot{\phi}\sin\theta = f_2(\theta,\phi) + \alpha f_1(\theta,\phi),$$

with

$$f_1(\theta,\phi) = -H_K\sin\theta\sin\phi\cos\phi - H_a\sin(\phi-\beta) + a_j\sin\theta,$$
$$f_2(\theta,\phi) = H_K\sin\theta\cos\theta\cos^2\phi + H_a\cos\theta\cos(\phi-\beta) + 4\pi M_S\sin\theta\cos\theta. \quad (3)$$

By inspection of Eq. (3), the IP equilibrium states are at the equator of the unit sphere,[18] i.e., $\theta_e = \pi/2$, for small injection current and applied field. Therefore, substitution of $\theta = \pi/2$ in Eq. (3) and integration of $f_1(\phi)$ (Ref. 35) lead to the one-dimensional effective energy density function $E_{\text{eff}}(\phi)$ for the IP equilibrium points:

$$E_{\text{eff}}(\phi) = -\tfrac{1}{2}H_K\cos^2\phi - H_a\cos(\phi-\beta) - a_j\phi$$
$$= -\tfrac{1}{2}H_K\cos^2\phi - H_x\cos\phi - H_y\sin\phi - a_j\phi, \quad (4)$$

where $\phi\in[0,2\pi]$. The locus of the critical points in the field plane (i.e., x-y plane) is obtain from the critical equilibrium conditions $\partial E_{\text{eff}}/\partial\phi = 0$ and $\partial^2 E_{\text{eff}}/\partial\phi^2 = 0$, where

$$\frac{\partial E_{\text{eff}}}{\partial\phi} = \frac{1}{2}H_K\sin 2\phi + H_x\sin\phi - H_y\cos\phi - a_j = 0 \quad (5)$$

and

$$\frac{\partial^2 E_{\text{eff}}}{\partial\phi^2} = H_K\cos 2\phi + H_x\cos\phi + H_y\sin\phi = 0. \quad (6)$$

The stable condition is then $\partial^2 E_{\text{eff}}/\partial\phi^2 > 0$. Therefore, the parametric forms of the locus of the critical fields are

$$H_x = -H_K\cos^3\phi + a_j\sin\phi,$$
$$H_y = H_K\sin^3\phi - a_j\cos\phi. \quad (7)$$

The above parametric forms will construct a modified SW astroid within the plane of the IP bias field from the influences of the STT. The astroid curve separates the regions where the free energy has two minima from the region where the energy has only one or no minimum. If $a_j = 0$, Eq. (7) leads to the original SW astroid of the uniaxial anisotropy case. For a uniaxial anisotropy with a saturation magnetization $M_S = 1000$ emu/cm^3, examples of various strengths of STT are plotted in Fig. 2. If the strength of the STT is smaller than the critical value, $a_c = H_K/2$, which is required to switch the magnetization at zero-bias field, the astroid stretches along the diagonal direction and compresses along the antidiagonal direction [see Figs. 2(a) and 2(b)]. Figure 2(a) is a SW astorid without the effect of the STT. Within this range of injected spin-polarized current, the switching mechanism of magnetization gradually changes for the distortion of the astroid as increasing the injecting current.

By introducing the method of the orientation of the critical curve proposed by Slonczewski[28] and Thiaville,[29] the tangent line of the locus in the parametric point ϕ is described by Eq. (5), and its direction is along the same direction of equilibrium magnetization $\mathbf{m}$. One can recognize the equation (6)

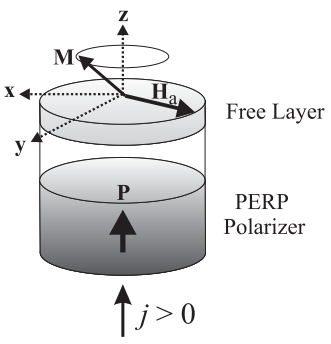

FIG. 1. Schematics of a spin valve with a perpendicular polarizer $\mathbf{p}$ and an in-plane (x-y plane) bias magnetic field $\mathbf{H}_a$. The easy axis of the free-layer magnetization $\mathbf{M}$ is along the $+x$ direction. The positive current j flows from the polarizer to the free layer.

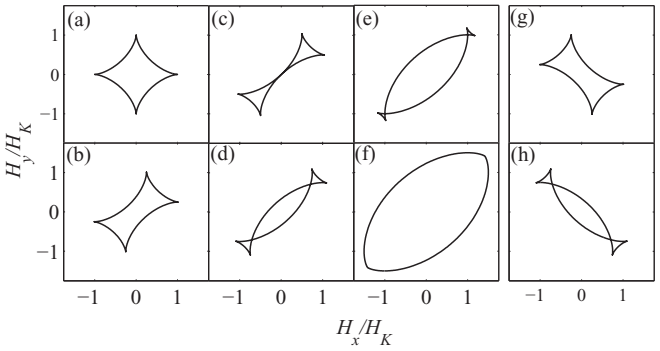

FIG. 2. The modified astroids for varying strengths of STT: (a) $a_j = 0$, (b) $a_j = H_K/4$, (c) $a_j = H_K/2$, (d) $a_j = 3H_K/4$, (e) $a_j = H_K$, (f) $a_j = 3H_K/2$, (g) $a_j = -H_K/4$, and (h) $a_j = -3H_K/4$.

of a straight line perpendicular to the tangent line, and this line divides the plane into two half planes. In one half plane the magnetization is in a stable condition and in the other half plane the magnetization is unstable. Therefore, it has two stable equilibrium states when the applied field is inside the modified astroid [see $\mathbf{H}_1$ in Fig. 3(a) and $\mathbf{H}$ in Figs. 3(b) and 3(c)], while only one stable equilibrium state when the applied field is outside the astroid [see $\mathbf{H}_2$ in Fig. 3(a) and $\mathbf{H}$ in Fig. 3(d)]. For $a_j < a_c$, the IP stable equilibrium will rotate around the z axis by varying the strengths of the STT.[18] This is even more clearly seen in Figs. 3(a) and 3(b), which also plot the directions of the equilibrium states (see the blue and red lines). For example, if $a_j = 0$ and $(H_x, H_y) = (0,0)$ [see Fig. 3(a)], there are two tangent lines (blue solid lines) along the easy axis, which correspond to the two stable states $(\phi_0^+ = 0^\circ, \phi_0^- = 180^\circ)$ at the easy axis, and two tangent lines (red dashed lines) along the hard axis, which correspond to the two unstable states at the hard axis. But if $a_j > 0$ $(j > 0)$ and $(H_x, H_y) = (0,0)$ [see Fig. 3(b)], we can inspect that the two stable states (ϕ^+, ϕ^-), which are the extensions of (ϕ_0^+, ϕ_0^-) for a finite STT, rotate counterclockwise away from the easy axis, and the two unstable states rotate clockwise away from

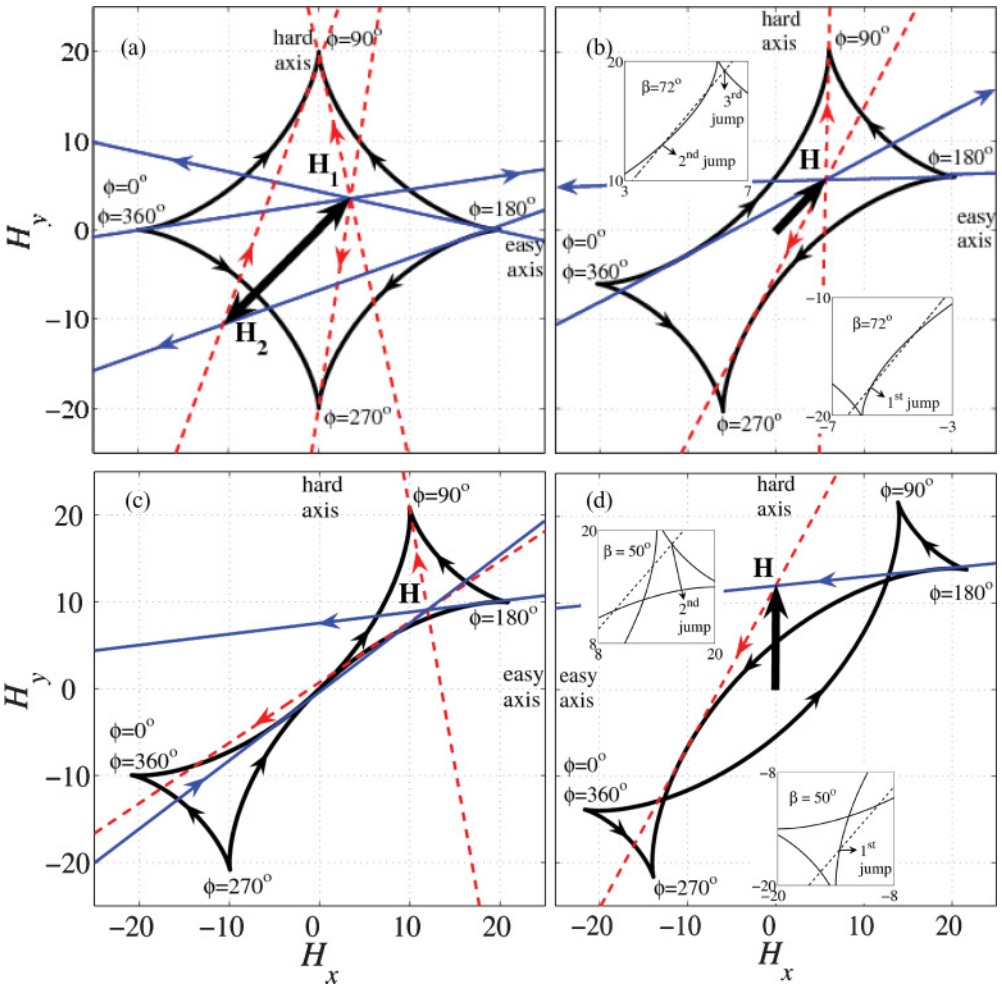

FIG. 3. (Color online) The oriented two-dimensional critical curve for uniaxial anisotropy $H_K = 20$ Oe and different strengths of STT: (a) $a_j = 0$, (b) $a_j = 6$ Oe, (c) $a_j = 10$ Oe, and (d) $a_j = 14$ Oe. The stable and unstable magnetization directions are shown by solid and dashed lines separately under a fixed IP field $\mathbf{H}$. Lower inset in (b): The first discontinuous jump of the state of the magnetization. Upper inset in (b): The second and third discontinuous jumps of the state of the magnetization. The dashed line is the orientation of the IP field, which makes an angle $\beta = 72^\circ$ with the easy axis. Lower inset in (d): The first discontinuous jump of the state of the magnetization. Upper inset in (d): The second discontinuous jump of the state of the magnetization. The dashed line is the orientation of the IP field, which makes an angle $\beta = 50^\circ$ with the easy axis.

the hard axis. According to the injected current direction, the IP rotation of (ϕ^+,ϕ^-) can be either clockwise as $j < 0$ or counterclockwise as $j > 0$. The IP rotation by the four equilibrium states means that the STT is driving the original magnetization out of the local energy minima $[(\phi_0^+,\phi_0^-)]$. However, if $H_a \neq 0$, the perpendicular component H_y (say, >0) can make ϕ^+ and ϕ^- start to rotate counterclockwise and clockwise, respectively [see Fig. 3(a)]. The combined effect of the STT and IP bias field can make ϕ^+ rotate to a larger angle than the rotation angle of ϕ^- [see **H** in Fig. 3(b)]. When the applied field is restricted to vary along one arbitrary chosen orientation, multiple discontinuous jumps possibly may appear. In particular, when the orientation of the IP field is specified to be near the cusp of the hard axis for $a_j < a_c$, there are always triple discontinuous jumps between the two stable equilibrium states, as shown in the upper left-hand inset and lower right-hand inset of Fig. 3(b) for a deviation angle $\beta = 72^\circ$ between the IP field and easy axis.

For $a_j = a_c$, two branches of the locus would intersect at (0,0) on the IP field plane, as shown in Fig. 2(c). From Eqs. (5) and (6), we can easily find that there are two possible equilibrium states at the field point (0,0), but they are indeed the inflection points of the effective energy. Therefore, the two stable states (ϕ^+,ϕ^-) are destroyed by the STT and there is no stable state at the point (0,0), and the magnetization would always precess, which is corresponding to the reported steady-state out-of-plane precessions (OPPs).[13–16] However, this steady-state precessional conclusion only exists for the zero IP field and cannot appear with a finite IP field. With a finite strength of the IP field, from analyzing the orientation of the critical curve, there are still two stable states inside the triangle region and one stable state outside the triangle region, as shown in Fig. 3(c). When the spin-torque strength is in the interval $a_c < a_j < a_{c2}$, where $a_{c2} \approx \alpha(4\pi M_S + H_K/2)$ is the critical STT of an out-of-plane stable state,[16,18] as shown in Figs. 2(d) and 2(e), the locus becomes a fishlike shape, and there is no stable equilibrium state in the fish-body region, which means there are infinite numbers of precessional states in this region. Actually, when the magnetic field is applied and its strength is within this region, there is no line going through the field point and is tangent to the constraint curves, and no stable equilibrium found. Similarly, by analyzing the orientation of the critical curve, there are two stable states inside the triangle region and one stable state outside the region, as shown in Fig. 3(d). In particular, when the IP field is orientated from $\beta = 45^\circ$ to the cusp of the hard axis for $a_j \geqslant a_c$, there are always double discontinuous jumps between the two stable equilibrium states, as shown in the upper left-hand inset and lower right-hand inset of Fig. 3(d) for a deviation angle $\beta = 50^\circ$ between the IP field and easy axis. It is worth noting that when $a_j \gtrsim 1.5H_K$, as shown in Fig. 2(f), the triangle region disappears and there is no bistable-state region, and only precessional and monostable states exist inside and outside the elliptical region, respectively.

It should be noted that when a_j is negative $(j < 0)$, the astroid would stretch along the antidiagonal direction and compress along the diagonal direction [see Figs. 2(g) and 2(h)], which is contrary to the case for positive a_j [see Figs. 2(a)–2(f)].

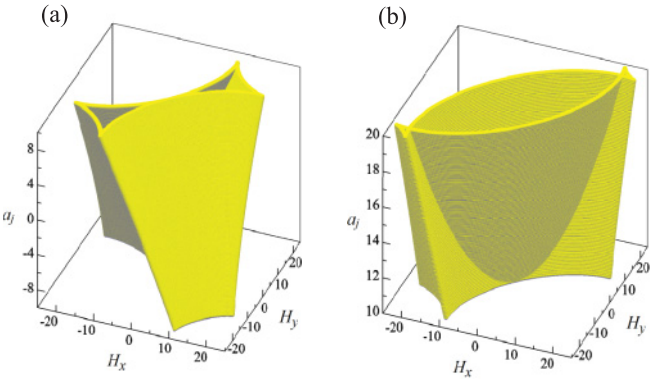

FIG. 4. (Color online) The three-dimensional critical surfaces of the instability conditions for (a) $-a_c < a_j < a_c$ and (b) $a_c < a_j < a_{c2}$ with $H_K = 20$ Oe.

A three-dimensional critical surface is shown in Fig. 4 with different strengths of the STT. In the range of $-a_c < a_j < a_c$, as shown in Fig. 4(a), the magnetization becomes unstable on the surface, while in the other range of $a_c < a_j < a_{c2}$, as shown in Fig. 4(b), the magnetization would be a steady precessional state within the body of the fishlike region.

III. CRITICAL FIELD

Three different critical fields are calculated: nucleation field, coercive force, and precessional critical field. In the following calculation, typical magnetic parameters of $M_S = 1000$ emu/cm^3 and $H_K = 20$ Oe, and $\alpha = 0.02$ are used. The angular dependence of the nucleation field, coercive force, and precessional critical field for a given strength of a STT are shown in Fig. 5.

A. Nucleation field

The nucleation field H_N is defined as the magnetic field at which there is a discontinuous jump of the free-layer magnetization. From Eq. (4) and the equilibrium condition, the nucleation field under the effect of a STT satisfies the simultaneous equations

$$H_N = -\frac{H_K \cos 2\phi}{\cos(\phi - \beta)}, \qquad H_N = \frac{a_j - \frac{1}{2}H_K \sin 2\phi}{\sin(\phi - \beta)}, \tag{8}$$

where $\beta \in [0,\pi]$.

1. Nucleation field when $a_j < H_K/2$

For various strengths of a STT, $a_j < a_c$, the numerical solutions of $H_N(a_j,\beta)$ as a function of the applied field angle in Eq. (8) are shown in Fig. 5(a). The smallest nucleation field for each a_j occurs when the orientation of the applied field is along 135° to the $+x$ axis, as shown in Fig. 5(a). It should be noted that the nucleation field had a local minimum at 0° with the effect of the STT, which is very different from the SW particle, where it is a local maximum. Also obvious from Fig. 5(a) is that the $H_N(a_j \neq 0,\beta)$ has triple solutions around the second cusp, and it corresponds to the multiple discontinuous jumps we have mentioned in Sec. II [see the inset in Fig. 3(b)].

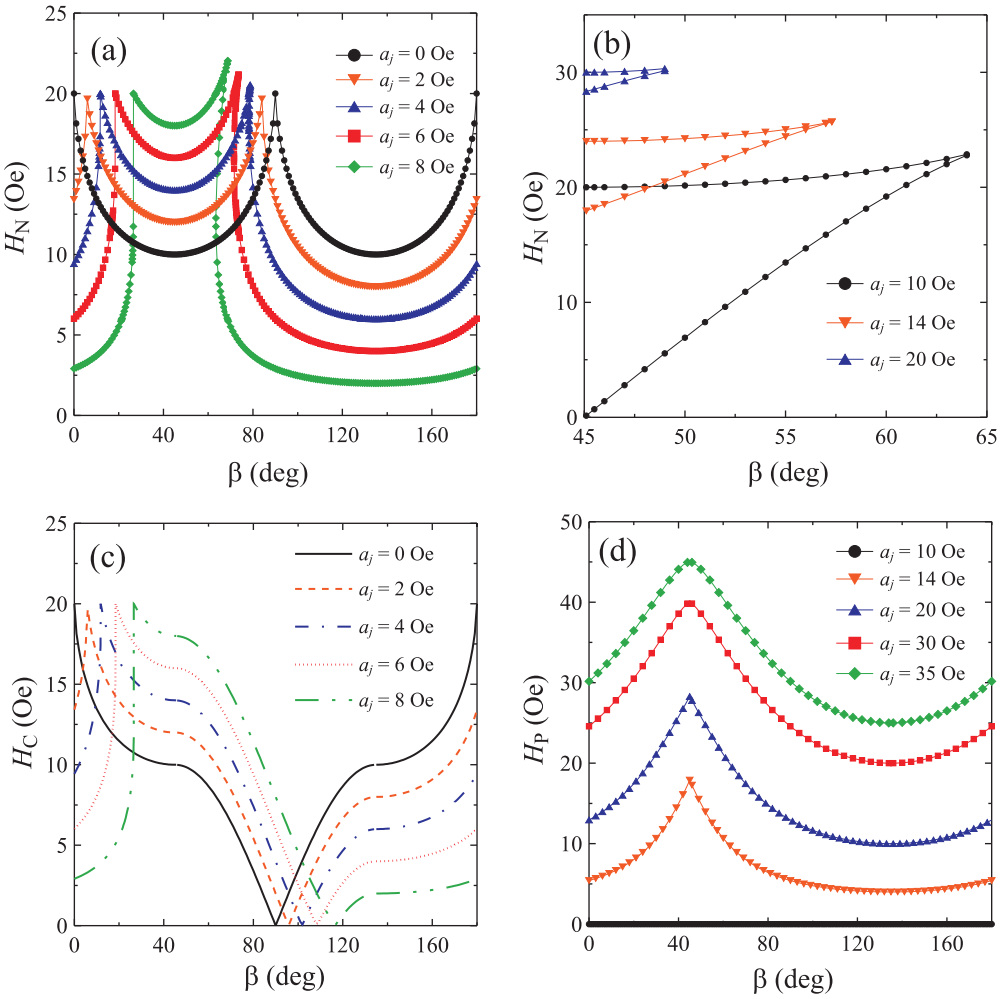

FIG. 5. (Color online) Calculated angular dependence of the critical fields for $H_K = 20$ Oe. (a) $H_N(a_j,\beta)$ vs applied field angle for various strengths of the STT, $a_j < a_c$. (b) $H_N(a_j,\beta)$ vs applied field angle for various strengths of the STT, $a_j > a_c$. (c) $H_C(a_j,\beta)$ vs applied field angle for various strengths of the STT, $a_j < a_c$. (d) $H_P(a_j,\beta)$ vs applied field angle for various strengths of the STT, $a_j > a_c$.

2. *Nucleation field when $a_j \geqslant H_K/2$*

When the strength of the STT is larger than the critical STT a_c and is smaller than the value $1.5H_K$, the bistable-state region can appear in the field space, as illustrated in Figs. 2(c)–2(e). The nucleation field for the discontinuous jump of the magnetization from one stable state to another one in this case can be calculated from Eq. (8). Figure 5(b) illustrates the double solutions for $H_N(a_j,\beta)$ versus field angle β for various a_j. The double values of H_N mean that there are two discontinuous jumps for the magnetization switching, which we have mentioned in the Sec. II [see the inset in Fig. 3(d)]. The angle for the double nucleation ranges from 45° to the angle for the hard-axis cusp of the astroid. When $a_j \geqslant 1.5H_K$, the double-nucleation phenomenon disappears.

B. Coercive force

The coercivity is defined as the magnetic field at which the projection of the magnetization onto the applied field direction is zero. From Eq. (8), and $\mathbf{H}_C \cdot \mathbf{m} = 0$ at the coercive field $\mathbf{H}_C$,[36] we can obtain

$$\begin{aligned} H_C &= \pm(a_j - H_K \sin\phi\cos\phi) \\ &= \pm(a_j + H_K \sin\beta\cos\beta). \end{aligned} \tag{9}$$

By considering the stability condition, we find that $\cos 2\beta_c < 0$ and β_c equals 45° or 135°. For $\beta \leqslant 45°$ or $\beta \geqslant 135°$, there is no stable solution with $\mathbf{H}_C \cdot \mathbf{m} = 0$. Therefore, the coercivity is

$$\begin{aligned} H_C &= \pm(a_j + H_K \sin\beta\cos\beta), \quad \pi/4 < \beta < 3\pi/4, \\ &= H_N, \quad \beta \leqslant \pi/4 \text{ or } \beta \geqslant 3\pi/4. \end{aligned} \tag{10}$$

The calculated angular dependence of coercivity $H_C(a_j,\beta)$ for various strengths of the STT, $a_j < a_c$, was shown at Fig. 5(c). From the Eq. (10), it is easy to show that if the deviation angle satisfies $\sin 2\beta_0 = -2a_j/H_K$ and $\cos 2\beta_0 = -\sqrt{1-(2a_j/H_K)^2}$, the coercivity is always zero. In Fig. 5(c), we only take the absolute values of the coercivity. Actually, the coercivity is negative when the deviation angle ranges from the angle at which the nucleation field is maximum

to angle β_0. This fact can also be observed in the following hysteresis behaviors, and will be discussed in detail in the next section.

C. Precessional critical field

For $a_c \leqslant a_j < a_{c2}$, precessional states will appear in the field space [see Figs. 2(c)–2(f)]. The maximal critical field $H_P(a_j \geqslant H_K/2,\beta)$ for the steady-precessional states can be calculated numerically from Eq. (8). Its functional dependences on the applied field angle for various strengths of the STT are plotted in Fig. 5(d). The maximum value of H_P for a given a_j is always at an angle of 45°, and the minimum one is at an angle of 135°. In particular, H_P is always zero as $a_j = a_c$, which is shown as the black dot in Fig. 5(d).

IV. HYSTERESIS BEHAVIOR WITH SPIN TORQUE

The hysteresis loop comprises two branches of the magnetization projection along the direction of the bias field. The descending branch is from the positive saturated magnetization and the ascending branch is from the negative saturated magnetization, and the magnetization switches between two branches when nucleation occurs. Figure 6 shows the macrospin-simulated results of hysteresis loops of the free layer under the effects of the IP magnetic field and the STT. The switching curves are characterized by the cosine of the angle between the free-layer magnetization and IP bias field, i.e., $m_H = \cos(\phi - \beta)$. The saturation magnetization, the uniaxial anisotropy field, and the damping constant are taken as $M_S = 1000$ emu/cm^3, $H_K = 20$ Oe, and $\alpha = 0.02$, respectively.

Figures 6(a)–6(c) show the hysteresis behaviors for $a_j = 6$ Oe ($<a_c$). When the deviation angle between the IP field and anisotropy axis is smaller than 45° and is larger than 135°, the nucleation field and coercivity will be the same, as illustrated in Figs. 6(a) and 6(c), and it follows the prediction of Eq. (10). In particular, from Fig. 6(a), the square hysteresis can only appear at a deviation angle of ∼18° instead of 0° without the STT.[36] This can be easily understood from the modified astroid. Because the STT influences the astroid and also the IP rotation of (ϕ^+,ϕ^-), the hysteresis behavior also follows and would not shift along the x axis even when the applied field is along the x axis. When the deviated angle ranges between 45° and 135°, the nucleation field and coercivity are different. In fact, this can be derived easily from Eq. (10). It suggests that the magnetization projection along the field direction is negative even before the instability of the magnetization occurs at a descending branch of the hysteresis loop. For the ascending branch, a similar behavior of magnetization appears within the range of 45° and 135°. In Fig. 6(b), as the angle ranges from 72° to 108°, the positive nucleation field and the negative coercive force are owing to the exchange of the ascending and descending branches at nucleation. This range of angle follows our prediction in Sec. III [dotted line, Fig. 5(b)]. Interesting behavior occurs around the deviated angle 72°. When the applied field sweeps from a positive value to a negative value, there are three discontinuous jumps switching back and forth between the descending and the ascending branches. The first

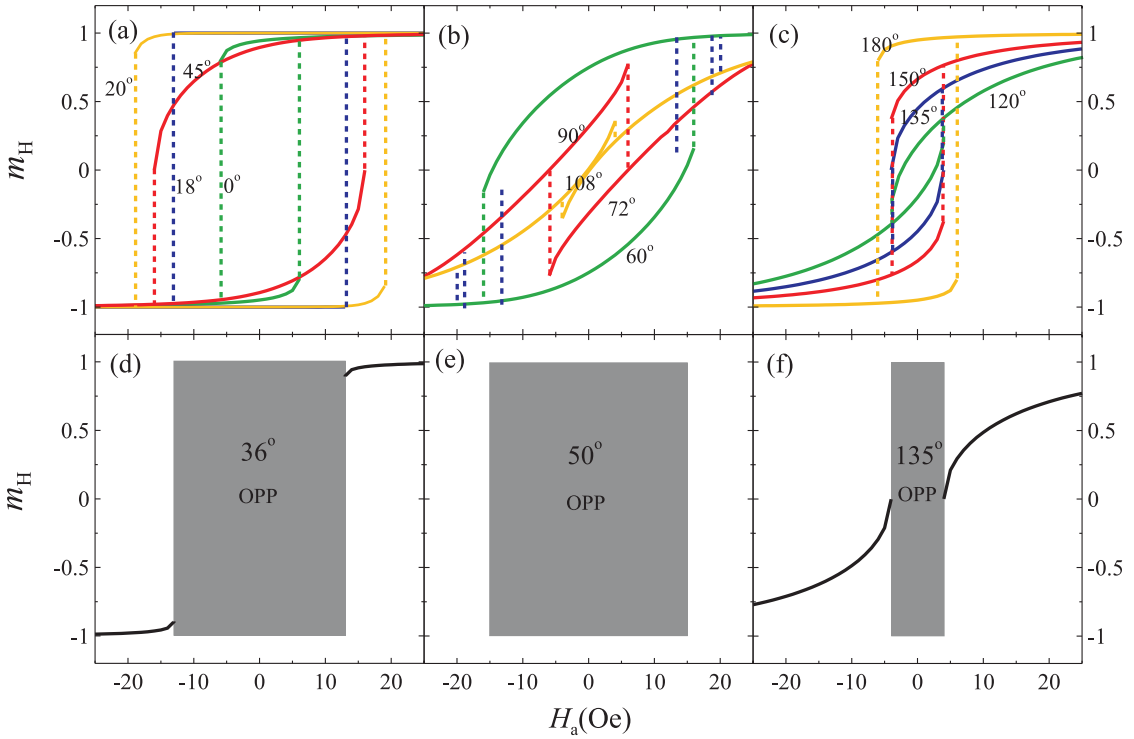

FIG. 6. (Color online) Hysteresis loops of the projective magnetization $m_H = \cos(\phi - \beta)$ for various orientations of the IP bias field and strengths of the STT: (a)–(c) $a_j = 6$ Oe, (d)–(f) $a_j = 14$ Oe. The shaded region denotes the OPP state. The numbers in all the figures denote the values of the angle β.

nucleation field is ∼18 Oe and magnetization jumps from the descending branch to the ascending branch. When the applied field further reduces to −14 Oe, the magnetization jumps back to the descending branch and stays at the same branch until the applied field equals −21 Oe. The magnetization nucleates to the ascending branch again beyond −21 Oe. Three transitions between the ascending and descending branches result from three nucleation fields within angles of ∼71.5°–73.5° [green curve, Fig. 5(a)]. The behavior of the hysteresis for this range is quite different from the hysteresis without the effect of the STT. Without the STT, the hysteresis with multiple discontinuous jumps can never be observed. The descending and the ascending branches of the hysteresis will intersect at a field angle of 108° at the zero-bias field [Fig. 6(b)], which corresponds to the zero coercivity predicted by our analytical result [Fig. 5(b)]. Until the IP bias field angle shifts further to 120°, a crossover of the hysteresis branches is never observed, and the hysteresis become normal again when $\beta \geqslant 120°$.

Figures 6(d)–6(f) illustrate the hysteresis loops for $a_j = 14$ Oe ($>a_c$). When $a_j > a_c$, the hysteresis loops show some OPP states (shaded in gray). The OPP region is almost square for an arbitrary orientation of the IP bias field because the magnetization goes into a large-angle precession.[18] The boundaries of the OPP region agree with our predictions for the maximal critical field H_P [see Fig. 5(c)]. In particular, when the bias field with $\beta = 50°$ sweeps from a positive value to a negative value, there are two discontinuous jumps switching back and forth between the descending and the ascending branches [see Fig. 6(e)]. One jump is at a negative nucleation field, and another one is at a positive nucleation field. The absolute values of the two nucleation fields follow our prediction in Sec. II [orange curve, Fig. 5(d)].

V. SUMMARY

Here we have identified a parametric form of the instability conditions with the IP magnetic field and also the PERP-STT. We presented studies on the influences of the STT on the conventional astroid and their geometrical determination of the stable magnetization. In addition to the regions with stable magnetizations, we also found that some steady states of the precessional state exist at certain values of the STT. We also calculate the nucleation, coercivity, precessional critical fields, and their dependence on the deviated angle from the anisotropy axis with the injected STT. We noted that the square hysteresis loop can only exist at a small deviated angle for the modification of the STT. Also the triple- and double-nucleation hysteresis loops can be observed at certain regions of the deviated angles for $a_j < a_c$ and $a_j > a_c$, respectively. Our results provide an easy and useful way to determine graphically the switching criteria and also the threshold of the precessional dynamical mode from the modified astroid. The modified astroid shall be very useful for designing STT spintronics devices, especially for spin-torque oscillators.[15]

ACKNOWLEDGMENT

The authors were supported by NSC 98-2112-M-002-012-MY3 and MOEA 98-EC-17-A-08-S1-006.

*d95222013@ntu.edu.tw
†crchang@phys.ntu.edu.tw

[1] J. A. Katine, F. J. Albert, R. A. Buhrman, E. B. Myers, and D. C. Ralph, Phys. Rev. Lett. **84**, 3149 (2000).
[2] E. B. Myers, F. J. Albert, J. C. Sankey, E. Bonet, R. A. Buhrman, and D. C. Ralph, Phys. Rev. Lett. **89**, 196801 (2002).
[3] S. I. Kiselev, J. C. Sankey, I. N. Krivirotov, N. C. Emley, R. J. Schoelkopf, R. A. Buhrman, and D. C. Ralph, Nature (London) **425**, 380 (2003).
[4] S. I. Kiselev, J. C. Sankey, I. N. Krivorotov, N. C. Emley, M. Rinkoski, C. Perez, R. A. Buhrman, and D. C. Ralph, Phys. Rev. Lett. **93**, 036601 (2004).
[5] W. H. Rippard, M. R. Pufall, S. Kaka, T. J. Silva, and S. E. Russek, Phys. Rev. B **70**, 100406(R) (2004).
[6] W. H. Rippard, M. R. Pufall, S. Kaka, S. E. Russek, and T. J. Silva, Phys. Rev. Lett. **92**, 027201 (2004).
[7] S. Kaka, M. R. Pufall, W. H. Rippard, T. J. Silva, S. E. Russek, and J. A. Katine, Nature (London) **437**, 389 (2005).
[8] F. B. Mancoff. N. D. Rizzo, B. N. Engel, and S. Tehrani, Nature (London) **437**, 393 (2005).
[9] W. H. Rippard, M. R. Pufall, S. Kaka, T. J. Silva, S. E. Russek, and J. A. Katine, Phys. Rev. Lett. **95**, 067203 (2005).
[10] A. Deac, K. J. Lee, Y. Liu, O. Redon, M. Li, P. Wang, J. P. Nozieres, and B. Dieny, Phys. Rev. B **73**, 064414 (2006).
[11] M. R. Pufall, W. H. Rippard, S. Kaka, T. J. Silva, and S. E. Russek, Appl. Phys. Lett. **86**, 082506 (2005).
[12] A. D. Kent, Nat. Mater. **6**, 399 (2007).
[13] A. D. Kent, B. Özyilmaz, and E. del Barco, Appl. Phys. Lett. **84**, 3897 (2004).
[14] K. J. Lee, O. Redon, and B. Dieny, Appl. Phys. Lett. **86**, 022505 (2005).
[15] D. Houssameddine, U. Ebels, B. Delaët, B. Rodmacq, I. Firastrau, F. Ponthenier, M. Brunet, C. Thirion, J.-P. Michel, L. Prejbeanu-Buda, M.-C. Cyrille, O. Redon, and B. Diney, Nat. Mater. **6**, 447 (2007).
[16] H. Morise and S. Nakamura, Phys. Rev. B **71**, 014439 (2005).
[17] H. Morise and S. Nakamura, J. Magn. Magn. Mater. **306**, 260 (2006).
[18] U. Ebels, D. Houssameddine, I. Firastrau, D. Gusakova, C. Thirion, B. Dieny, and L. D. Buda-Prejbeanu, Phy. Rev. B **78**, 024436 (2008).
[19] J. C. Sankey, Y.-T. Cui, J. Z. Sun, J. C. Slonczewski, R. A. Buhrman, and D. C. Ralph, Nat. Phys. **4**, 67 (2008).
[20] C. Heiliger and M. D. Stiles, Phys. Rev. Lett. **100**, 186805 (2008).
[21] P. M. Haney, C. Heiliger, and M. D. Stiles, Phys. Rev. B **79**, 054405 (2009).
[22] C. Wang, Y.-T. Cui, J. Z. Sun, J. A. Katine, R. A. Buhrman, and D. C. Ralph, Phys. Rev. B **79**, 224416 (2009).
[23] J. C. Slonczewski, J. Magn. Magn. Mater. **159**, L1 (1996).
[24] L. Berger, Phys. Rev. B **54**, 9353 (1996).
[25] E. H. Frei, S. Shtrikman, and Treves, Phys. Rev. **106**, 446 (1957).
[26] A. Aharoni, J. Appl. Phys. **30**, 70 (1959).
[27] E. C. Stoner and E. P. Wohlfarth, Philos. Trans. R. Soc. London A **240**, 599 (1948); IEEE Trans. Magn. **27**, 3475 (1991).

[28]J. C. Slonczewski, Research Memorandum No. RM 003.111.224 (IBM Research Center, Poughkeepsie, NY, 1956) (unpublished).
[29]A. Thiaville, J. Magn. Magn. Mater. **182**, 5 (1998).
[30]C. R. Chang and J. S. Yang, Phys. Rev. B **54**, 11957 (1996).
[31]J. Z. Sun, Phys. Rev. B **62**, 570 (2000).
[32]Y. Henry, S. Mangin, J. Cucchiara, J. A. Katine, and E. E. Fullerton, Phys. Rev. B **79**, 214422 (2009).
[33]Z. Li and S. Zhang, Phys. Rev. B **69**, 134416 (2004).
[34]A. N. Slavin and V. S. Tiberkevich, Phys. Rev. B **72**, 094428 (2005).
[35]J. Miltat, G. Albuquerque, and A. Thiaville, in *Spin Dynamics in Confined Magnetic Structures I*, edited by B. Hillebrands and K. Ounadjela (Springer, Berlin, 2001).
[36]C. R. Chang, J. Appl. Phys. **69**, 2431 (1991).